

Ab initio calculation of ionization potential and electron affinity in solid-state organic semiconductors

Youngho Kang,¹ Sang Ho Jeon,² Youngmi Cho,² and Seungwu Han^{1,*}

¹*Department of Materials Science and Engineering and Research Institute of Advanced Materials, Seoul National University, Seoul 151-755, Korea*

²*CAE Team, Samsung Display Co., Ltd, 95 Samsung 2-ro, Giheung-gu, Yongin-City, Gyeonggi-Do 446-711, Korea*

(Received 26 July 2015; revised manuscript received 16 December 2015; published 22 January 2016)

We investigate the vertical ionization potential (IP) and electron affinity (EA) of organic semiconductors in the solid state that govern the optoelectrical property of organic devices using a fully *ab initio* way. The present method combines the density functional theory and many-body perturbation theory based on *GW* approximations. To demonstrate the accuracy of this approach, we carry out calculations on several prototypical organic molecules. Since IP and EA depend on the molecular orientation at the surface, the molecular geometry of the surface is explicitly considered through the slab model. The computed IP and EA are in reasonable and consistent agreements with spectroscopic data on organic surfaces with various molecular arrangements. However, the transport gaps are slightly underestimated in calculations, which can be explained by different screening effects between surface and bulk regions.

DOI: [10.1103/PhysRevB.93.035131](https://doi.org/10.1103/PhysRevB.93.035131)

I. INTRODUCTION

The organic semiconductors based on π -conjugated molecules are widely used in various applications such as organic thin-film transistors (OTFTs), organic photovoltaics (OPV), and organic light-emitting diodes (OLEDs) [1–6]. Compared to inorganic counterparts, the organic molecules have several advantages such as low cost, easy fabrication, and mechanical flexibility [7–9]. Thus, devices based on organic semiconductors have been steadily improved and have started to enter into the mainstream markets in optics and electronics [10–13].

In every organic device, one of the key factors that governs device efficiency is the energy position of frontier orbitals [14]. For example, the difference in the ionization potential (IP) and electron affinity (EA) between two adjacent organic films corresponds to the energy barrier against the hole and electron transports, respectively, that determine the current levels of organic devices [15]. Therefore, prediction of IP and EA as well as their alignments among different organic solids is the key to the efficient material selection in multilayered organic devices.

In isolated molecules, the energy levels of orbitals are mainly determined by hybridization between atomic orbitals of constituent elements. In solid states, on the other hand, the polarization of surrounding medium in response to addition and removal of the electron significantly influences the orbital levels. As a consequence, it reduces the difference between IP and EA, the so-called transport gap ($E_t = \text{IP} - \text{EA}$) of organic solids by 1–2 eV from the energy gap between the highest-occupied-molecular orbital (HOMO) and the lowest-unoccupied-molecular orbital (LUMO) in the single molecule [16]. Thus, it is critical to take into account the polarization effect to predict the positions of the molecular energy levels in solid-state systems with high precision.

The polarization energies for HOMO and LUMO (P_+ and P_- , respectively) are formally defined by the difference of IP and EA in solid states and gas phases, respectively:

$$P_+ = \text{IP}_{\text{solid}} - \text{IP}_{\text{gas}}, \quad (1a)$$

$$P_- = \text{EA}_{\text{gas}} - \text{EA}_{\text{solid}}. \quad (1b)$$

Several theoretical methods have been proposed to evaluate $P_{+(-)}$. They include polarizable continuum model (PCM) [17], classical microelectrostatic model (CMM) using polarizable force field method [18,19], and quantum-mechanics-molecular-mechanics (QM/MM) techniques [20,21]. PCM is a simplified electrostatic model that approximates the screening with the polarizable medium. A previous study using the PCM method showed that it can describe the variation of the polarization energy with respect to the type of molecules reasonably [17]. However, this method usually assumes isotropic dielectric constants and neglects the orientation in the molecular packing. As such, it could not capture the asymmetric nature of polarization energies between P_+ and P_- that is clearly seen in experiment [18,20].

The CMM model splits the electrostatic energy into the nuclear relaxation energy, multipole interactions, and charge-induced dipole interactions [18,19]. In this scheme, atom-centered multipoles and their polarizabilities are obtained by *ab initio* calculations for an isolated molecule. The total electrostatic energy is then determined by counting all the pairwise interactions within the polarizable force field. Hence, it inherently takes into account the influence of molecular packing style on the polarization energy. Ryno *et al.* reported the asymmetric $P_{+(-)}$ of oligoacene series by using this method [18]. However, the result of this method hinges on the employed atomistic models, implying that it does not always guarantee the accuracy comparable to *ab initio* calculations. For example, the molecular quadrupole moment of the polarizable force field did not reproduce that of quantum calculation for the perfluorinated species [18].

*hansw@snu.ac.kr

In the case of QM/MM calculations, the main idea is to separate a large chemical system into a small region with quantum-mechanical description and its surrounding that is treated by classical dynamics. Several QM/MM studies were carried out on the polarization effect in polymer and organic solids [20,21]. However, similar to CMM, the results of QM/MM approach significantly depend on the charge model employed in the MM region. For instance, it was reported that QM/MM calculation with a charge fluctuation model results in larger P_- than P_+ for oligoacene molecular crystals on the contrary to experiment, due to the lack of higher-order polarization energy arising from the interaction between multipoles and induced dipoles [20].

On the other hand, several *ab initio* quantum mechanical methods have also been proposed to calculate IP and EA of organic materials with reasonable accuracy and computation cost. For example, in optimally tuned range-separated hybrid (otRSH) functional method, the Coulomb interaction between electrons is partitioned into long- and short-range parts using error functions [22,23]. The parameters for range separation and the fraction of short-range Fock exchange are determined in a self-consistent way by enforcing Koopmans theorem and derivative discontinuity. This functional accurately reproduces the molecular energy levels for isolated molecules and computed HOMO/LUMO levels are in good agreements with the experimental IP and EA values [22,23].

As an extension of otRSH, they proposed in Ref. [24] screened RSH in which the screening effect in solids is reflected by adjusting the fraction of the long-range Fock energy in inverse proportion to the static dielectric constant. It was shown that this approach well reproduces the HOMO-LUMO gap of molecules in solid state. Since the RSH functional provides HOMO-LUMO gaps for single molecule as well as solid state, the polarization energies were estimated in Ref. [24] by assuming $P_+ = P_-$. While the screened RSH method fully considers the molecular geometry in solid state, such an assumption for the polarization energy still neglects the detailed dielectric response.

Another quantum-mechanical approach is to employ the *GW* approximation that can evaluate the quasiparticle (QP) levels without any adjustable parameters. It was shown that the *GW* method can precisely predict IP and EA of various isolated molecules [25–27]. In addition, some studies demonstrated that *GW* calculations reproduce the spectroscopic features of organic materials in solid state with a fair accuracy [28,29]. However, full determination of IP and EA of organic solids has not been demonstrated with the *GW* method as far as we are aware.

In this study, using a full-blown *ab initio* method combining density functional theory (DFT) and many-body *GW* methods, we calculate IP and EA of organic crystals with certain surface orientations. Since our goal is to evaluate IP and EA rather than E_i , which was the focus of the previous *GW* studies [28,29], the relative positions of the QP levels from *GW* calculations should be redefined with respect to the vacuum level. To accomplish that, we calculate the average electrostatic potential and vacuum level from slab models using the DFT method. The positions of the QP levels below the vacuum level are then determined by aligning the average electrostatic potentials between the solid and the

bulk region in the slab. Such an approach has been widely used in evaluating the work function of solid surfaces [30]. Compared to previous methods for calculating IP and EA, the advantage of the present method is to evaluate IP and EA without any parameters. In addition, while most of previous studies did not consider the vacuum level shift associated with the molecular arrangement at the surface, the present scheme explicitly addresses its impact on IP and EA. To test validity, we apply the method to prototypical π -conjugated organic semiconductors; pentacene (PEN), copper phthalocyanine (CuPC), 3,4,9,10-perylene-dicarboxylicdianhydride (PTCDA), tris(8-hydroxy-quinoline)-aluminum (Alq3), and *N,N'*-diphenyl-*N,N'*-bis(1-naphthyl)-1,1' biphenyl-4,4'' diamine (α -NPD) and quantitatively compare calculated HOMO and LUMO levels with experimental data.

II. METHODS

A. Computational setup

To perform the DFT and *GW* calculation, we employed the Vienna *ab initio* simulation package (VASP) code [31]. The PBE-based generalized gradient approximation (GGA) functional is used for the exchange-correlation energy [32]. The cutoff energy for plane-wave basis set is 400 eV. The selected molecules are known to be polymorphic and we choose the space groups of PEN [33], CuPC [34], PTCDA [35], Alq3 [36], and α -NPD [37] as P-1, P1, P21/c, P-1, and P-1, respectively. Figure 1 shows the crystal structures of computed organic solids. The lattice parameters and internal coordinates of molecules are fixed to the experimental data because the GGA functional lacks the long-range London dispersion force that is essential for the intermolecular structure.

To obtain the QP energies that correspond to the vertical excitation energy for adding or removing an electron, the many-body-perturbation theory based on the *GW* approximation is employed. In *GW* approximations, the QP energy ($E_{n\vec{k}}^{\text{QP}}$) of an orbital is perturbatively calculated based on the wave function ($\psi_{n\vec{k}}$) and eigenvalue ($E_{n\vec{k}}$) obtained from the DFT calculations:

$$E_{n\vec{k}} = \text{Re}[\langle \psi_{n\vec{k}} | T + V_{\text{ion}} + V_{\text{H}} + \Sigma(E_{n\vec{k}}) | \psi_{n\vec{k}} \rangle], \quad (2)$$

where T , V_{ion} , and V_{H} are the kinetic energy operator, the ionic potential, and the Hartree potential, respectively. In Eq. (2), Σ is the energy-dependent self-energy operator and it is formulated as follows within the *GW* approximation:

$$\Sigma(\vec{r}, \vec{r}', E) = \frac{i}{4\pi} \int_{-\infty}^{\infty} e^{i\omega'\delta} G(\vec{r}, \vec{r}', E + E') W(\vec{r}, \vec{r}', E') dE', \quad (3)$$

where G , W , and δ represent the Green's function and the screened Coulomb interaction, and an infinitesimal, respectively. Optical dielectric constant for calculating screened Coulomb interaction, W , is evaluated in random-phase approximation [38,39].

Various levels of self-consistency for $E_{n\vec{k}}^{\text{QP}}$ calculation are defined depending on whether $\psi_{n\vec{k}}$ and $E_{n\vec{k}}$ for calculating G and W are updated for self-consistency or not [40,41]. In this study, we carried out G_0W_0 calculation where $\psi_{n\vec{k}}$ and $E_{n\vec{k}}^{\text{QP}}$

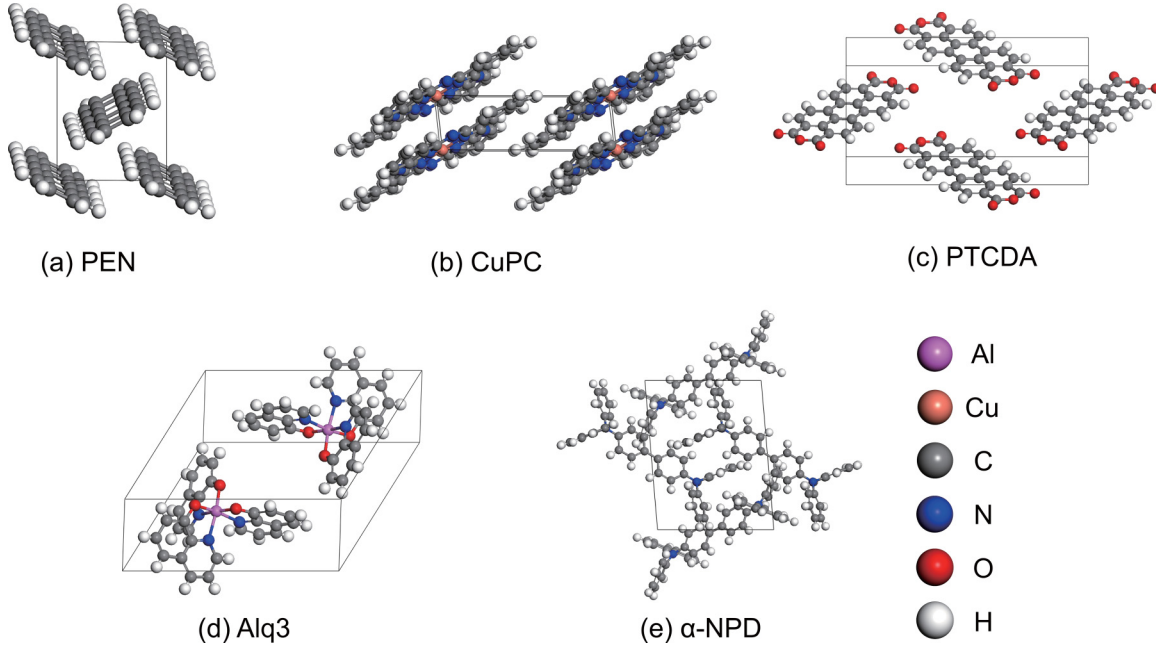


FIG. 1. Crystal structures of (a) PEN, (b) CuPC, (c) PTCDA, (d) Alq3, and (e) α -NPD.

are fixed to DFT results for testing computational parameters such as \vec{k} -point mesh and the number of the empty bands (N_{em}). Since G_0W_0 calculation tends to underestimate the IP and E_t of an isolated molecule and further update of QP levels improves agreement between calculation and experiment [25–27,29], the final electronic structures are obtained by the GW_0 method in which $E_{n\vec{k}}$ in G is updated. This method is also known to be a consistent way to estimate the accurate band gaps in inorganic materials [40,41].

We tested the \vec{k} -point mesh and N_{em} to ensure the convergence of each $E_{n\vec{k}}^{QP}$ of G_0W_0 calculation within 0.1 eV. We emphasize that as long as the bulk calculation is concerned, only the differences between $E_{n\vec{k}}^{QP}$'s are physically meaningful as everything is defined up to an arbitrary potential. However, as we determine the reference point of the electrostatic potential through the slab calculation (see the next subsection), and use it to evaluate IP and EA, individual $E_{n\vec{k}}^{QP}$'s have independent physical meaning. Therefore, the convergence of $E_{n\vec{k}}^{QP}$, not E_t , is more important in the present study. The selected \vec{k} -point mesh for GW calculation are Γ -centered $2 \times 2 \times 1$, $1 \times 5 \times 1$, $3 \times 1 \times 1$, $3 \times 1 \times 1$, and $1 \times 1 \times 1$ for PEN, CuPC, PTCDA, Alq3, and α -NPD, respectively.

The convergence test with regard to N_{em} showed that E_t 's for all the tested materials are relatively insensitive to N_{em} and hundreds of N_{em} are sufficient, which is consistent with previous GW studies on organic materials [28,29]. In contrast, we find that $E_{n\vec{k}}^{QP}$ converges slowly with respect to N_{em} and even with thousands of N_{em} , the convergence is not arrived yet. This implies that the use of N_{em} ensuring the convergence of E_t is not enough to investigate IP and EA and the convergence of N_{em} should be tested more thoroughly. Slow convergence behaviors of $E_{n\vec{k}}^{QP}$ were also found in previous GW calculations on single molecules [42]. Therefore, we use 2778 (PEN), 2603 (CuPC), 3380 (PTCDA), 3358 (Alq3), and 3302 (α -NPD) of

N_{em} and remaining errors are corrected by fitting the computed data to the equation of $E_{n\vec{k}}^{QP} = a/N_{em} + b$ and extrapolating to the case of $N_{em} \rightarrow \infty$ as shown in Fig. 2. The data fit is performed using the last four points of N_{em} and it is seen that the extrapolation is critical to achieve the accuracy within 0.1 eV.

B. Calculation of IP and EA

To calculate IP and EA of a molecular solid, first we determine the averaged HOMO and LUMO levels in solid state that correspond to the positions of first peaks in density of state (DOS), $\bar{\epsilon}_{HOMO}^{PBE}$, and $\bar{\epsilon}_{LUMO}^{PBE}$, as shown in Fig. 3(a). The use of peak positions instead of edge levels facilitates the comparison of IP and EA with experiment, since the peak positions in the spectroscopic data are defined more clearly than edge positions [16]. The quasiparticle shifts of HOMO and LUMO with respect to PBE levels ($\Delta\bar{\epsilon}_{HOMO}$ and $\Delta\bar{\epsilon}_{LUMO}$) are then evaluated as follows:

$$\Delta\bar{\epsilon}_{HOMO} = \bar{\epsilon}_{HOMO}^{GW_0} - \bar{\epsilon}_{HOMO}^{PBE}, \quad (4a)$$

$$\Delta\bar{\epsilon}_{LUMO} = \bar{\epsilon}_{LUMO}^{GW_0} - \bar{\epsilon}_{LUMO}^{PBE}. \quad (4b)$$

Since the GW_0 and PBE calculations share the same electrostatic potential, the energy level shifts are well defined by Eq. (4).

As a next step, we calculate the mean electrostatic potential in the slab with the Miller index of (hkl) (\bar{V}_{core}^{slab}) by averaging the Coulomb potential at the atomic sites of molecules in the bulk region [see Fig. 3(b)]. $\Delta V(hkl)$ denotes the difference between \bar{V}_{core}^{slab} and vacuum level. We also calculate \bar{V}_{core}^{bulk} for crystal structures in a similar way to \bar{V}_{core}^{slab} . This is used in aligning energy levels in surface and bulk calculations. Finally, surface-dependent IP and EA are obtained via the equations

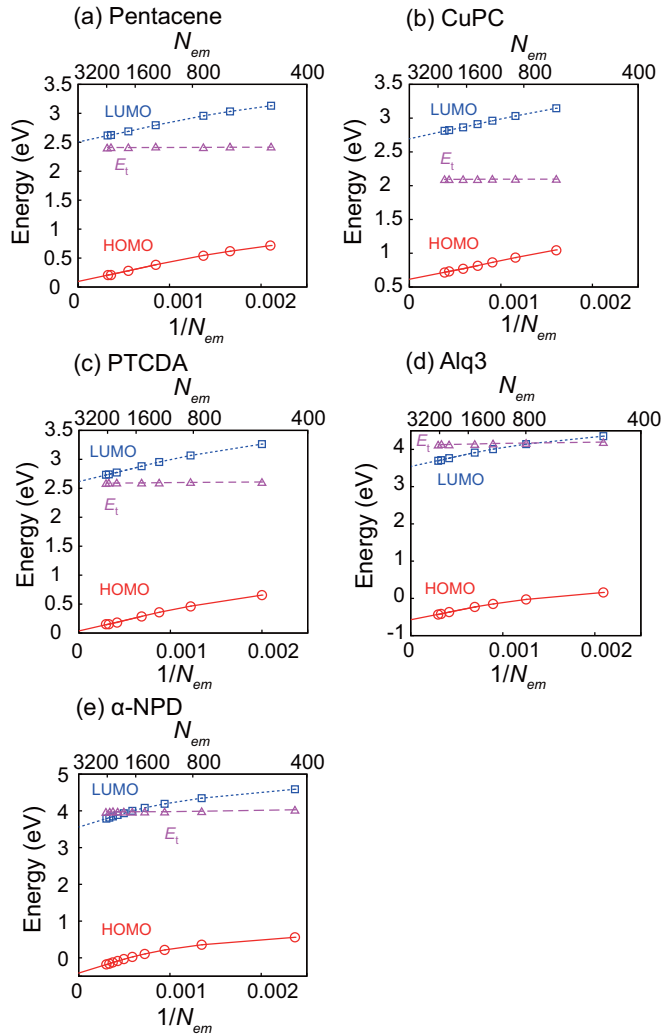


FIG. 2. Convergence of G_0W_0 quasiparticle energies of HOMO (circle) and LUMO (square) and the transport gap (triangle) with respect to the number of unoccupied states.

below:

$$\text{IP} = \Delta V(\text{hkl}) - [\bar{\epsilon}_{\text{HOMO}}^{\text{PBE}} + \Delta\bar{\epsilon}_{\text{HOMO}} - \bar{V}_{\text{core}}^{\text{bulk}}], \quad (5a)$$

$$\text{EA} = \Delta V(\text{hkl}) - [\bar{\epsilon}_{\text{LUMO}}^{\text{PBE}} + \Delta\bar{\epsilon}_{\text{LUMO}} - \bar{V}_{\text{core}}^{\text{bulk}}]. \quad (5b)$$

III. RESULTS AND DISCUSSIONS

GW calculations provide the quasiparticle energy levels that correspond to the experimental photoemission spectroscopic data. Figure 4 compares the density of states (DOS) from GW calculations with available UPS/IPES experimental data [16,43]. (We adjust the first peaks of UPS and IPES by 0.2 ~ 0.4 eV to match calculated HOMO and LUMO levels, respectively, due to the gap difference between calculations and experiments [29], which will be discussed in the below.) The calculated DOSs are broadened with Gaussian functions and the broadening widths are 0.25, 0.4, 0.6, 0.5, and 0.4 eV for PEN, CuPC, PTCDA, Alq3, and α -NPD, respectively. The broadening implicitly reflects the effects of the finite tem-

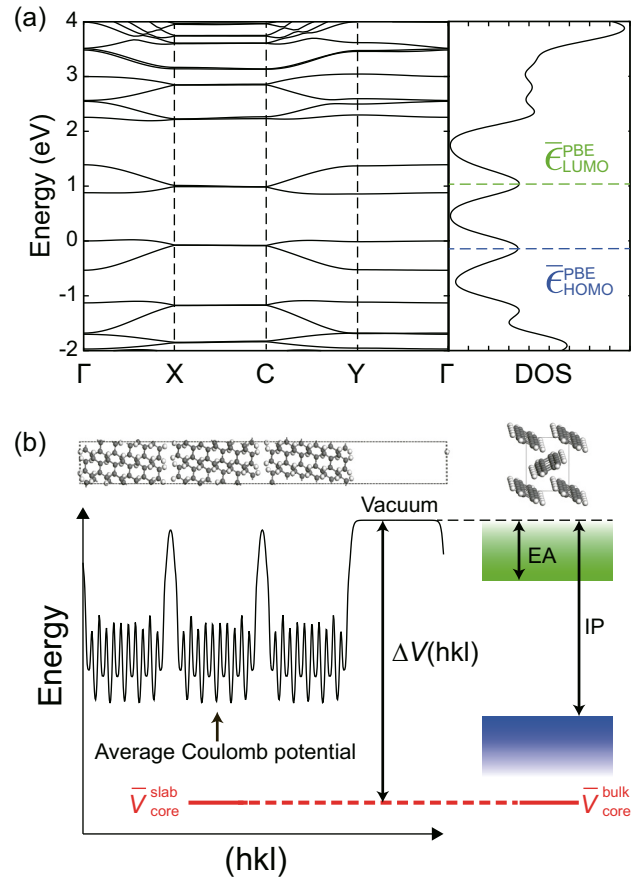


FIG. 3. (a) The band structure and DOS of PEN in solid state from PBE calculations. The Fermi level is set to zero. $\bar{\epsilon}_{\text{HOMO}}^{\text{PBE}}$ and $\bar{\epsilon}_{\text{LUMO}}^{\text{PBE}}$ are DOS-based average values of HOMO and LUMO levels. (b) The schematic for obtaining IP and EA from the surface model with the orientation of (hkl). The solid line is the Coulomb potential ($V_C = V_{\text{ion}} + V_{\text{H}}$) averaged over in-plane directions. $\bar{V}_{\text{core}}^{\text{slab}}$ and $\bar{V}_{\text{core}}^{\text{bulk}}$ are averaged V_C at the atomic sites that belong to bulk molecules in slab and bulk calculations, respectively. $\Delta V(\text{hkl})$ indicates the difference between the vacuum levels and $\bar{V}_{\text{core}}^{\text{slab}}$.

perature, disordered molecular arrangement, and the limited resolution of the measurement technique. As shown in Fig. 4, the relative energy positions of the frontier orbital near HOMO and LUMO from the present calculations match well with UPS/IPES spectrum within 0.2 eV.

The calculated IP and EA of molecular solids with different surface orientations are displayed in Fig. 5. Experimentally, the specific surface orientation of the grown sample is not clearly given but the rough arrangement of molecules such as standing-up or flat-lying could be confirmed for planar molecules such as PEN [44,45], CuPC [46], and PTCDA [16,47]. Therefore, we assume the specific surface orientations that reflect experimental molecular arrangements. (The adopted molecular geometries are shown in Fig. S1 of the Supplemental Material [48].) Two types of the molecular arrangements for PEN and CuPC are found: one is flat-lying configuration and the other is the standing-up arrangement. As shown in Fig. 5, in the case of PEN and CuPC, the calculations for the standing-up configurations result in lower (higher) IP (EA) than those of flat-lying configurations,

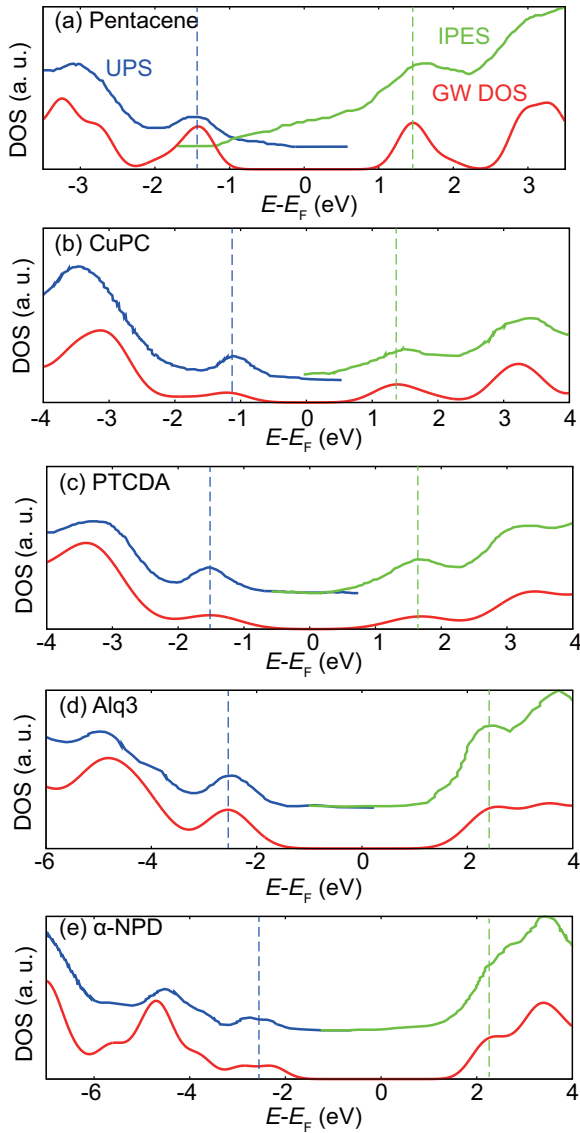


FIG. 4. Comparison between calculated DOS and experimental spectra [16,43]. Computed DOSs are broadened by Gaussian function with 0.25, 0.4, 0.6, 0.5, and 0.4 eV of widths for PEN, CuPC, PTCDA, Alq3, and α -NPD, respectively. Vertical dashed lines are the positions of HOMO (blue) and LUMO (green). All the spectra are adjusted such that zero is at the middle of the transport gap. Due to the difference in the transport gap, the first peaks of UPS and IPES data in experiments are shifted by 0.26, 0.27, 0.40, 0.15, and 0.30 eV for PEN, CuPC, PTCDA, Alq3, and α -NPD, respectively.

well reproducing the variation of IPs in experiment. This is because positive hydrogen ions exposed at the edge of surface molecules effectively lower the vacuum level in the standing-up configuration.

In contrast to PEN and CuPC, flat-lying configurations were found for PTCDA. We employ two molecular surfaces that are close to flat-lying configurations: (100) and $(\bar{1}02)$ surfaces that exhibit $\sim 30^\circ$ and $\sim 8^\circ$ angles between long axis of a molecule and xy plane, respectively, and it is found that IP (EA) of (100) surface is 0.3 eV larger (smaller) than that of $(\bar{1}02)$. In both directions, the computed HOMO-LUMO pairs lie within the

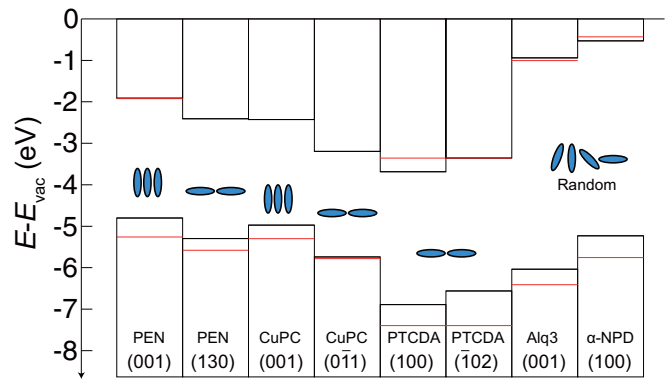


FIG. 5. The calculated IP and EA of molecular solids with different surface orientations (black solid lines). Red lines denote the experimental data of corresponding organic materials and blue ellipses indicate the schematic molecular orientation at the surface in experiment. For the fair comparison, we refer to the first peak positions of occupied and unoccupied states in UPS/IPES data [16,44–46].

experimental range. On the other hand, we select nondipolar surface for the calculation of Alq3 and α -NPD because their complex 3D structures often favor films with the amorphous structures [49].

In the above, it was demonstrated that the present method predicts IP and EA of organic semiconductors reasonably. However, IP and EA positions, and consequently E_t , are slightly wider in experiment, as can be seen in Fig. 5 and Table I. This is in part because the UPS/IPES experiments are sensitive to the electronic characters of molecules at the surface [50] where the polarization effect is reduced because of nearby vacuum. In the calculation, the transport gaps are estimated for the bulk in which a molecule is fully surrounded by other molecules. Therefore, the polarization effect inside bulk is larger compared to the surface [29]. To confirm this further, we evaluate E_t^{gas} of an isolated molecule in gas phase using oTSH functional in the last column of Table I [51]. It is seen that the experimental transport gaps always lie between the solid and gas phase values. Hence, the agreement between theory and experiment can be improved by full GW calculations on surface models, which will be computationally more expensive than the present approach. We also note that

TABLE I. The theoretical transport gaps of organic semiconductors in gas and bulk phases. The theoretical values for gas and bulk phases are obtained by using oTSH functional and GW_0 calculation, respectively. The experimental values are peak-to-peak gaps of surface sensitive UPS and IPES data. The discrepancy between theory and experiment is mainly attributed to the overestimate of bulk gap in experiment.

	Solid	Experiment	Gas
PEN	2.89	3.42 [43], 3.33 [45]	4.95
CuPC	2.55	3.10 [16,49]	4.57
PTCDA	3.21	4.00 [16], 4.05 [47], 3.80 [49]	5.14
Alq3	5.10	5.40 [16], 5.50 [49]	6.40
α -NPD	4.70	5.30 [16]	5.74

according to Ref. [29], the incomplete screening at the surface can only partly account for the red shift in theory and other factors such as finite temperature and final state vibrational effects can give rise to the additional shifts.

As was discussed in the Introduction, there exist several theoretical methods for calculating IP and EA, but most of them do not consider surface effects explicitly [17,18,20,21]. As a result, the previous models are not appropriate in explaining the surface dependence of IP and EA found in experiments. In the present approach, the vacuum level shifts due to the electrostatic effect of the surface geometry originating from inequivalent charge distribution at the molecular edge [52], and IP and EA for pentacene and CuPC differ by $0.5 \sim 0.8$ eV depending on the surface orientation.

Furthermore, the PCM method results in nearly identical P_+ and P_- since it employs isotropic dielectric constant and neglects characteristic molecular packing. For example, P_+ and P_- of PEN from the PCM method were -1.10 and -1.15 eV, respectively, while the experimental values are -1.63 and -1.17 eV on average [18]. This also means that PCM is not able to address the difference among various polymorphs with distinct molecular arrangements. In our calculation, by contrast, P_+ and P_- averaged over two surface directions are -1.69 (-1.45) and -0.79 (-0.60) eV with respect to IP and EA of gas phase in the experiment (otRSH calculation), showing better agreements with experiment than the PCM results. This is because the present method explicitly takes into account the molecular structure and dielectric anisotropy. Our results also imply that the specific arrangements of the molecules plays an important role in determination of IP and EA of organic semiconductors and this cannot be achieved by the continuum models.

IV. SUMMARY AND CONCLUSION

In conclusion, we carried out a fully *ab initio* calculation to evaluate IP and EA of organic materials in solid state using the *GW* method in combination with DFT calculations.

We found that the convergence of QP levels with respect to the virtual states is important to estimate IP and EA accurately. The present method well captures the dependence of IP and EA on the surface geometry for linear or planar molecules. Furthermore, it was shown that the level alignments among tested molecules in solid state are in reasonable and consistent agreements with experimental data even though the transport gaps in calculation are slightly smaller than those in experiment due to different polarization effects between bulk and surface, which limits direct comparison with experimental results. We also showed the importance of the molecular packing effects for the determination of IP and EA via demonstrating inequivalent polarization energies of HOMO and LUMO for PEN, which cannot be addressed by the continuum models like PCM.

On the computational side, the advantage of the present method is that the computation is relatively straightforward and does not require any parameter-fitting that is necessary in every other empirical approaches. In addition, the computational cost is only modest. For example, the present *GW* calculations for each organic solid took ~ 5 h on average with 32 computational cores. Therefore, we believe that the present method can be efficiently applied to a wide range of organic solids, thereby allowing for fast material screening in organic devices.

ACKNOWLEDGMENTS

This research was supported by Samsung Display, EDISON program, through the Ministry of Science, ICT, and Future Planning, National Research Foundation of Korea (NRF-Grant No. 2012M3C1A6035307), and the Future Semiconductor Device Technology Development Program (Grant No. 10052925), funded by the Ministry of Trade, Industry, and Energy (MOTIE) and the Korea Semiconductor Research Consortium (KSRC). The computations were performed at the KISTI supercomputing center (Grant No. KSC-2014-C3-051).

-
- [1] S. R. Forrest, *Nature* **428**, 911 (2004).
 - [2] H. Ma, H.-L. Yip, F. Huang, and A. K.-Y. Jen, *Adv. Funct. Mater.* **20**, 1371 (2010).
 - [3] L.-L. Chua, J. Zaumseil, J.-F. Chang, E. C. W. Ou, P. K. H. Ho, H. Sirringhaus, and R. H. Friend, *Nature* **434**, 194 (2005).
 - [4] H. W. Lee, S. J. Lee, J. R. Koo, E. S. Cho, S. J. Kwon, W. Y. Kim, J. Park, and Y. K. Kim, *Electron. Mater. Lett.* **9**, 865 (2013).
 - [5] A. Hagfeldt and M. Graätzel, *Acc. Chem. Res.* **33**, 269 (2000).
 - [6] S. Reineke, F. Linder, G. Schwartz, N. Seidler, K. Walzer, B. Lüssem, and K. Leo, *Nature* **459**, 234 (2009).
 - [7] M. Muccini, *Nat. Mater.* **5**, 605 (2006).
 - [8] J. A. Rogers, Z. Bao, A. Makhija, and P. Braun, *Adv. Mater.* **9**, 741 (1999).
 - [9] T. Sekitani, U. Zschieschang, H. Klauk, and T. Someya, *Nat. Mater.* **9**, 1015 (2010).
 - [10] H. Uoyama, K. Goushi, K. Shizu, H. Nomura, and C. Adachi, *Nature* **492**, 234 (2012).
 - [11] N. Koumura, Z.-S. Wang, S. Mori, M. Miyashita, E. Suzuki, and K. Hara, *J. Am. Chem. Soc.* **128**, 14256 (2006).
 - [12] A. Hadipour, B. de Boer, and P. W. M. Blom, *Adv. Mater.* **18**, 169 (2008).
 - [13] M. G. Helander, Z. B. Wang, J. Qiu, M. T. Greiner, D. P. Puzzo, Z. W. Liu, and Z. H. Lu, *Science* **332**, 944 (2011).
 - [14] H. Ishii, K. Sugiyama, E. Ito, and K. Seki, *Adv. Mater.* **11**, 605 (1999).
 - [15] A. P. Kulkarni, C. J. Tonzola, A. Babel, and S. A. Jenekhe, *Chem. Mater.* **16**, 4556 (2004).
 - [16] I. G. Hill, A. Kahn, Z. G. Soos, and R. A. Pascal, Jr., *Chem. Phys. Lett.* **327**, 181 (2000).
 - [17] P. K. Nayak and N. Periasamy, *Organic Electronics* **10**, 1396 (2009).
 - [18] S. M. Ryno, S. R. Lee, J. S. Sears, C. Risko, and J.-L. Brédas, *J. Phys. Chem. C* **117**, 13853 (2013).
 - [19] C. Poelking, M. Tietze, C. Elschner, S. Olthof, D. Hertel, B. Baumeier, F. Würthner, K. Meerholz, K. Leo, and D. Andrienko, *Nat. Mater.* **14**, 434 (2015).
 - [20] J. E. Norton and J.-L. Brédas, *J. Am. Chem. Soc.* **130**, 12377 (2008).

- [21] S. Difley, L.-L. Wang, S. Yeganeh, S. R. Yost, and T. V. Voorhis, *Acc. Chem. Res.* **43**, 995 (2010).
- [22] T. Stein, H. Eisenberg, L. Kronik, and R. Baer, *Phys. Rev. Lett.* **105**, 266802 (2010).
- [23] S. Refaely-Abramson, S. Sharifzadeh, N. Govind, J. Autschbach, J. B. Neaton, R. Baer, and L. Kronik, *Phys. Rev. Lett.* **109**, 226405 (2012).
- [24] S. Refaely-Abramson, S. Sharifzadeh, M. Jain, R. Baer, J. B. Neaton, and L. Kronik, *Phys. Rev. B* **88**, 081204 (2013).
- [25] C. Rostgaard, K. W. Jacobsen, and K. S. Thygesen, *Phys. Rev. B* **81**, 085103 (2010).
- [26] F. Hüser, T. Olsen, and K. S. Thygesen, *Phys. Rev. B* **87**, 235132 (2013).
- [27] M. J. van Setten, F. Weigend, and F. Evers, *J. Chem. Theory Comput.* **9**, 232 (2013).
- [28] M. L. Tiago, J. E. Northrup, and S. G. Louie, *Phys. Rev. B* **67**, 115212 (2003).
- [29] S. Sharifzadeh, A. Biller, L. Kronik, and J. B. Neaton, *Phys. Rev. B* **85**, 125307 (2012).
- [30] C. J. Fall, N. Binggeli, and A. Baldereschi, *J. Phys. Condens. Matter* **11**, 2689 (1999).
- [31] G. Kresse and J. Furthmüller, *Phys. Rev. B* **54**, 11169 (1996).
- [32] J. P. Perdew, K. Burke, and M. Ernzerhof, *Phys. Rev. Lett.* **77**, 3865 (1996).
- [33] S. Schiefer, M. Huth, A. Dobrinevski, and B. Nickel, *J. Am. Chem. Soc.* **129**, 10316 (2007).
- [34] A. Hoshino, Y. Takenaka, and H. Miyaji, *Acta Crystallogr. Sect. B* **59**, 393 (2003).
- [35] K. Tojo and J. Mizuguchi, *Z. Kristallogr.* **217**, 255 (2002).
- [36] F. Suzuki, T. Fukushima, M. Fukuchi, and H. Kaji, *J. Phys. Chem. C* **117**, 18809 (2013).
- [37] J.-A. Cheng and P.-J. Cheng, *J. Chem. Crystallogr.* **40**, 557 (2010).
- [38] M. Shishkin and G. Kresse, *Phys. Rev. B* **74**, 035101 (2006).
- [39] G. Kang, Y. Kang, and S. Han, *Phys. Rev. B* **91**, 155141 (2015).
- [40] M. Shishkin, M. Marsman, and G. Kresse, *Phys. Rev. Lett.* **99**, 246403 (2007).
- [41] Y. Kang, G. Kang, H.-H. Nahm, S.-H. Cho, Y. S. Park, and S. Han, *Phys. Rev. B* **89**, 165130 (2014).
- [42] S. Sharifzadeh, I. Tamblyn, P. Doak, P. T. Darancet, and J. B. Neaton, *Eur. Phys. J. B* **85**, 323 (2012).
- [43] F. Amy, C. Chan, and A. Kahn, *Organic Electronics* **6**, 85 (2005).
- [44] H. Fukagawa, H. Yamane, T. Kataoka, S. Kera, M. Nakamura, K. Kudo, and N. Ueno, *Phys. Rev. B* **73**, 245310 (2006).
- [45] W. Han, H. Yoshida, N. Ueno, and S. Kera, *Appl. Phys. Lett.* **103**, 123303 (2013).
- [46] W. Chen, H. Huang, S. Chen, Y. L. Huang, X. Y. Gao, and A. T. S. Wee, *Chem. Mater.* **20**, 7017 (2008).
- [47] E. V. Tsiper, Z. G. Soos, W. Gao, and A. Kahn, *Chem. Phys. Lett.* **360**, 47 (2002).
- [48] See Supplemental Material at <http://link.aps.org/supplemental/10.1103/PhysRevB.93.035131> for the adopted molecular geometries.
- [49] S. Krause, M. B. Casu, A. Schöll, and E. Umbach, *New J. Phys.* **10**, 085001 (2008).
- [50] M. Bär, S. Nishiwaki, L. Weinhardt, S. Pookpanratana, O. Fuchs, M. Blum, W. Yang, J. D. Denlinger, W. N. Shafarman, and C. Heske, *Appl. Phys. Lett.* **93**, 244103 (2008).
- [51] To confirm the accuracy of the otRSH calculation, we compare calculated IPs of single molecules with experimentally reported ones. The experimental IPs of PEN, CuPC, PTCDA, and Alq3 are 6.7 [24], 6.38, 8.15, and 7.25 eV [16], which show good agreement with our calculation results of 6.41, 6.50, 8.13, and 7.05 eV within maximum error of ~5%.
- [52] G. Heimel, I. Salzmann, S. Duhm, and N. Koch, *Chem. Mater.* **23**, 359 (2011).